American Mineralogist, Volume 91, pages 1643–1656, 2006

An experimental study of the oxidation state of vanadium in spinel and basaltic melt with implications for the origin of planetary basalt

K. RIGHTER,[1,*] S.R. SUTTON,[2,3] M. NEWVILLE,[3] L. LE,[4] C.S SCHWANDT,[4] H. UCHIDA,[5] B. LAVINA,[6] AND R.T. DOWNS[5]

[1] Mailcode KT, NASA Johnson Space Center, 2101 NASA Parkway, Houston, Texas 77058, U.S.A.
[2] Department of the Geophysical Sciences, University of Chicago, 5734 S. Ellis Avenue, Chicago, Illinois 60637, U.S.A.
[3] GSECARS, University of Chicago, 5734 S. Ellis Ave., Chicago, Illinois 60637, U.S.A.
[4] Jacobs Sverdrup Engineering and Science, Houston, Texas 77058, U.S.A.
[5] Department of Geosciences, University of Arizona, Tucson, Arizona 85721, U.S.A.
[6] Dipartimento di Mineralogia e Petrologia, Università di Padova, Italy

ABSTRACT

The distribution of V in magmatic rocks is controlled primarily by spinel stability. Extensive previous experimental work at oxidized conditions on doped (V-rich) compositions has led to the recognition of the importance of temperature, oxygen fugacity, and spinel composition, but also left ambiguity with respect to the relative importance of these variables in controlling $D_V^{spinel/melt}$. One major uncertainty has been the valence of V in the spinel and glass. Spinel-melt pairs were equilibrated at low and variable oxygen fugacities, with a range of V and Ti contents. XANES spectra were measured on the spinel and glass products, and pre-edge peaks measured and calibrated against valence with the use of glass and oxide standards. The valence of V is always greater in the glass than in the spinels. In spinel, V is dominantly 3+ at oxygen fugacities near the FMQ (fayalite magnetite quartz) buffer, but we find evidence for mixed 3+, 4+, and 5+ at oxidized conditions (FMQ to air), and 2+ and 3+ at very reduced conditions [FMQ to IW-1 (1 $\log f_{O_2}$ unit below the iron wüstite buffer)]. Increased V contents in spinels are correlated with increased $D_V^{spinel\text{-}melt}$, at constant temperature and oxygen fugacity. However, increased Ti content causes only a slight decrease in $D_V^{spinel\text{-}melt}$ and a shift to more reduced V (smaller pre-edge peak), which may be related to Fe-V exchange equilibria. Using the new partition coefficients, together with published results and valence information, expressions have been derived to predict $D_V^{spinel/melt}$ for basaltic systems. Application of these expressions to natural suites illustrate their utility and also the great range of $D_V^{spinel/melt}$ values relevant to natural systems. Calculation of V depletions in planetary mantles from basalt suites must take silicate, oxide, and metal fractionation into account, as is demonstrated using terrestrial, lunar, martian, and eucritic samples.

Keywords: Vanadium, oxygen fugacity, basalt, spinel

INTRODUCTION

Spinel-structured oxides are common in magmatic rocks, both as an early phase during basaltic magma fractionation and late as titanomagnetite in evolved magmas. Because the spinel structure can accept a wide variety of transition metals, such as Fe^{2+}, Ni, Mn, Zn, Fe^{3+}, Ti, Cr, and V, there are complicated compositional variations that can be attributed to substitutions as well as temperature and oxygen fugacity (e.g., Roeder and Reynolds 1991; Maurel and Maurel 1983; Ariskin and Nikolaev 1996). Because spinels also are host phases for minor elements such as Ni, Co, Ru, Ir, and Rh, many experimental studies have aimed to predict partitioning behavior as a function of intensive variables such as T, f_{O_2}, and composition (Capobianco and Drake 1990; Capobianco et al. 1994; Nielsen et al. 1994; Horn et al. 1994; Righter et al. 2004, 2006).

Spinel can be a significant host phase for V, which has multiple oxidation states (V^{2+}, V^{3+}, V^{4+}, and V^{5+}) at oxygen fugacities relevant to natural systems. The magnitude of $D_V^{spinel/melt}$ is known to be a function of composition, temperature, and f_{O_2}, but the uncertainty of the oxidation state under the range of natural conditions has made elusive a thorough understanding of $D_V^{spinel/melt}$ (e.g., Fig. 1). For example, V^{3+} is likely to be stable in spinels, on the basis of exchange with Al in experiments in the CaO-MgO-Al_2O_3-SiO_2 system (Canil 1997). On the other hand, it has been argued that V^{4+} should be stable across the range of natural oxygen fugacities in nature (Borisov et al. 1987; Toplis and Corgne 2002). In some more reduced systems, V^{2+} may be present, such as in the solar nebula (e.g., Connolly and Burnett 2003). To build on our previous work in more oxidized systems (Righter et al. 2006), we have carried out new experiments to define better three aspects of $D_V^{spinel/melt}$ partitioning. First, we completed a series of experiments across a range of relatively reducing conditions from the FMQ buffer to 2 $\log f_{O_2}$ units below the IW buffer, with V present in the spinel at natural levels (~300 ppm V). Second, a series of experiments was completed with variable V contents and at two different oxygen fugacities—IW and FMQ. And third, a series of experiments was completed with variable Ti contents and at two different oxygen fugacities—IW and FMQ. Vanadium valence in glasses and spinels from these new experiments, as well as from more oxidized samples from previous studies, was determined

* E-mail: kevin.righter-1@nasa.gov

using micro-XANES at the Advanced Photon Source at Argonne National Laboratory. Use of the glass calibration curve of Sutton et al. (2005) for V in spinels was validated by confirming the similarity of spinel spectra in synthetic oxides of known valence and structural state. The new results are used, together with previous results, to understand the valence of V in spinel-melt systems across 12 orders of magnitude of oxygen fugacity and develop predictive expressions with application to natural systems.

Depletions of V in planetary mantles are traditionally attributed to separation of metal to form a metallic core. We use our new results for spinel together with data for other silicates, oxides, and metal/silicate partitioning studies, to discuss the causes of V depletions in planetary mantles. In particular, we weigh the relative importance of silicates, oxides, and metals in producing V depletions in the mantles of the Earth, Moon, Mars, and Vesta (EPB).

Experimental methods

Previous studies have highlighted the potential effects of Ti and V content on the magnitude of $D_V^{spinel/melt}$ (e.g., Righter et al. 2006; Toplis and Corgne 2002). However, it is ambiguous whether the variation is due to Ti or V content, melt composition, f_{O_2}, or temperature. Righter et al. (2006) showed f_{O_2}, T, and X effects, and highlighted the drawbacks of existing datasets to predict and understand D_V. To isolate the cause of the variation, a series of compositions were prepared that would yield variable spinel compositions by doping with Ti and V. Five compositions—undoped natural Hawaiian ankaramite, +1% V_2O_3, +5% V_2O_3, +5% TiO_2, and +10% TiO_2—were equilibrated at both the IW and FMQ buffers to investigate the effect of V and Ti; all compositions were doped with 1% Cr_2O_3 to promote spinel growth (e.g., Roeder and Reynolds 1991; Righter et al. 2004). A Hawaiian ankaramite was studied because it is primitive (11 wt% MgO) and has a composition that is similar to many natural systems such as OIB, MORB, arc, and planetary (martian, lunar, asteroidal) basalts.

These compositions were placed on either Re (f_{O_2} lower than FMQ), or Fe presaturated Pt (f_{O_2} higher than FMQ) wire loops in Deltech furnaces, with variable f_{O_2} at 1300 °C. The oxygen fugacity of individual experiments was controlled by mixing CO and CO_2 in a reference furnace at 1200 °C, where the desired emf was adjusted before introduction to the sample. The samples were held in the furnace hotspot for 2 to 5 days, and then quenched by rapid removal. All experimental samples contain spinel and glass (Fig. 2), and a few also contain olivine.

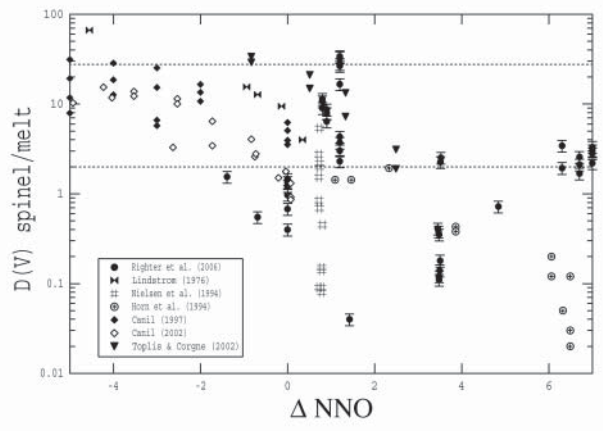

Figure 1. $D_V^{spinel/melt}$ vs. oxygen fugacity relative to the Ni-NiO buffer (ΔNNO) for many previous studies. There is an overall general trend of increasing D_V with decreasing oxygen fugacity, but the scatter at any given value of ΔNNO is due to other factors such as spinel major-element composition, or V or Ti content, temperature, and structure (normal or inverse). Data are from the studies of Righter et al. (2006), Lindstrom (1976), Nielsen et al. (1994), Horn et al. (1994), Canil (1997, 2002), and Toplis and Corgne (2002).

Three additional experiments were undertaken to produce V-bearing oxides as XANES standards to compare with glass calibrations produced by Sutton et al. (2005). $Mg_3V_2O_8$ and $Mg_2V_2O_7$, both of which contain V^{5+} (see below), were synthesized at 1 bar, 1300 °C, and oxygen fugacities equivalent to air, from mixtures of MgO and VO_2, (92004; Table 1). Nearly stoichiometric MgV_2O_4 spinel (see below) was synthesized at 1 bar, 1200 °C, and oxygen fugacity of the iron-wüstite (IW) buffer (62304 and 62504; Table 1), from mixtures of MgO and V_2O_3. A third experiment was performed at higher pressure in a piston-cylinder apparatus (PC1; Table 1). A double-capsule technique was employed where the inner Au capsule contained hematite and magnetite, and the outer Pt capsule contained 2MgO-VO_2 and the inner capsule. At 8 kb and 1250 °C, nearly stoichiometric Mg_2VO_4 was produced after 18 hours and an isobaric quench.

Analytical techniques

All major elements in spinels and glasses were analyzed with a CAMECA SX100 electron microprobe at NASA-JSC, using an accelerating voltage of 20 kV and sample current of 20 nA. Standards include both natural (kaersutite, wollastonite, chromite, rutile, olivine, rhodonite, potassium feldspar, albite) and synthetic (V metal, NiO) standard materials. Counting times for major elements were typically 10 s, and as long as 120 s for low concentrations of V in spinels and

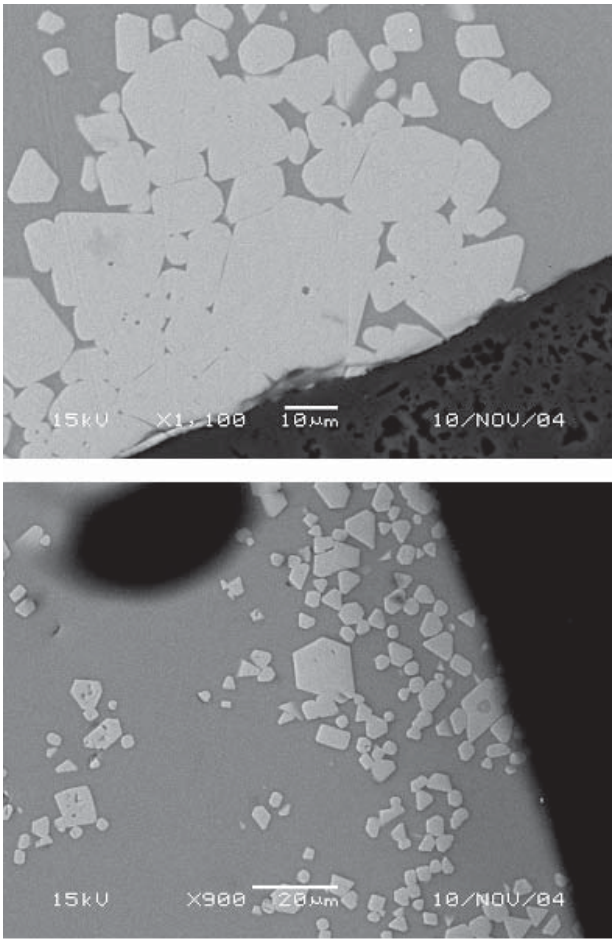

Figure 2. (**a**) Back-scattered electron image of chromian spinel grown from the ankaramite composition (doped with 5 wt% V_2O_3) at 1300 °C, log f_{O_2} = –10.58 (IW buffer), and equilibrated for 76 hours (Table 1). Light-gray phase is spinel, the darker-gray phase is glass, and the black regions are epoxy; scale bar is 10 µm. (**b**) Back-scattered electron image of chromian spinel grown from the ankaramite composition (undoped) at 1300 °C, log f_{O_2} = –8.22 (FMQ buffer), and equilibrated for 48 hours (Table 1). Light-gray phase is spinel, the darker-gray phase is glass, and the black regions are epoxy; scale bar is 20 µm.

TABLE 1. Summary of experimental conditions

Exp.	*T* (°C)	Reference log f_{O_2}*	Sample f_{O_2}*	ΔIW*	dopant	Time (h)	phases	$D_V^{sp/gl}$
FMQ	1300	–9.37, IW+2.53	–8.22	2.53	none	48	gl, sp	7.9
+1%V	1300	–9.37, IW+2.53	–8.22	2.53	1 wt% V_2O_3	48	gl, sp	8.1
+5%V	1300	–9.13, IW+2.78	–7.97	2.78	5 wt% V_2O_3	73	gl, sp	6.3
+5%Ti	1300	–8.94, IW+2.97	–7.78	2.97	5 wt% TiO_2	48	gl, sp	6.2
+10%Ti	1300	–8.94, IW+2.97	–7.78	2.97	10 wt% Cr_2O_3	48	gl, sp	5.5
IW+2	1300	–10.28, IW+1.63	–9.12	1.63	none	48	gl, sp	8.2
IW	1300	–12.30, IW–0.40	–11.15	–0.40	none	48	gl, sp	18.4
+1%V	1300	–12.30, IW–0.40	–11.15	–0.40	1 wt% V_2O_3	48	gl, sp	22.1
+5%V	1300	–12.30, IW–0.40	–11.15	–0.40	5 wt% V_2O_3	76	gl, sp	25.7
+5%Ti	1300	–12.29, IW–0.38	–11.13	–0.38	5 wt% TiO_2	72	gl, sp	18.8
+10%Ti	1300	–12.29, IW–0.38	–11.13	–0.38	10 wt% Cr_2O_3	72	gl, sp	19.8
IW-1	1300	–13.41, IW–1.51	–12.09	–1.51	none	51	gl, sp	17.5
IW-2	1300	–14.18, IW–2.27	–13.02	–2.27	none	64	gl	–
158B	1300	–	–1.65	+8.91	1 wt% Rh, Os, Cr	52	gl, sp	0.11
159A	1300	–	–6.49	+4.07	1 wt% Ru, Cr, Ni	49	gl, sp	2.5
159B	1300	–	–6.49	+4.07	1 wt% Rh, Os, Cr	49	gl, sp	3.1
162A	1300	–	–5.07	+5.49	1 wt% Ru, Cr, Ni	48	gl, sp	2.7
162B	1300	–	–5.07	+5.49	1 wt% Rh, Os, Cr	48	gl, sp	7.3
202	1250	–	–3.53	+7.60	–	31	g, sp	0.08
T5	1248	–	–6.45	+4.70	–	75	gl sp, ol	11.2
T6	1180	–	–0.91	+11.08	–	115	gl sp, ol	2.2
T11	1275	–	–5.98	+4.86	–	65	gl sp, ol	6.5
T13	1252	–	–0.68	+10.43	–	69	gl sp, ol	1.7
T14	1250	–	–6.00	+5.13	–	79	gl sp, ol	16.7
62304	1200	–	–11.74	0.0	–	48	MgV_2O_4	–
62504	1200	–	–11.74	0.0	–	48	MgV_2O_4	–
PC1	1250	–	–2.55	+9.19	–	18	Mg_2VO_4	–
92004	1300	–	–0.68	+9.88	–	92	$Mg_2V_2O_7$, $Mg_3V_2O_8$	–

* Oxygen fugacity was set in a reference cell at 1200 °C, and reported here as both an absolute and relative f_{O_2}. Oxygen fugacity of the sample is re-calculated for 1300 °C, relative to the buffer determinations of O'Neill 1987; IW = iron-wüstite buffer, and ΔIW refers to the oxygen fugacity of the sample relative to the IW buffer; sp = spinel structured oxide, ol = olivine, and gl = glass.

glasses. Under the latter conditions, detection limits were approximately 100 ppm for V. Interference of Ti*K*α on V*K*α peaks (Snetsinger et al. 1968) were avoided by counting Ti on PET using integral mode, and V on LiF in differential mode. PAP φ–ρ–Z corrections were used in the data reduction (Pouchou and Pichoir 1991). FeO and Fe_2O_3 in spinels were calculated by charge balance and stoichiometry (Carmichael 1967), and spinel compositions were calculated to 3 cations. All analyses are reported in Tables 2–4.

Single-crystal structures from each oxide synthesized as a standard were determined by X-ray diffraction (XRD) with the aim of identifying the phases and determine the valence states of V. Selected crystals include two spinels from experiments 62504 (1300 °C, IW buffer) and PC1 [1250 °C, 8 kbar, HM (hematite-magnetite) buffer] with compositions close to MgV_2O_4 and $Mg_{1.6}V_{1.4}O_4$, respectively, and a sample of $Mg_3(VO_4)_2$ from experiment 92004 (1300 °C, air). Data collections were performed with a Bruker X8 single-crystal X-ray diffractometer (Mo*K*α radiation, graphite monochromator) equipped with a CCD area detector. Details are included in Table 4. Structural refinements were carried out against f_{O_2} with SHELXL-97 (Sheldrick 1997) using both ionic and atomic scattering curves for O for spinels (62504a and PC1) and atomic scattering curves for $Mg_3(VO_4)_2$, to *wR*, a statistical measure of the refinement quality, ranging from 0.05 to 0.07. After XRD investigation, the same crystals were mounted on glass slides and polished for electron microprobe analysis (Table 5).

The lattice parameter of the spinel from experiment 62504, 8.4110(4) Å, is smaller than previously reported for stoichiometric MgV_2O_4, 8.431, 8.42, and 8.421 Å (Mamiya and Onoda 1995; Reuter et al. 1983; Rüdorff and Reuter 1947, respectively). Refined occupancies of the tetrahedral T and octahedral M sites indicate that they are not full, and some V^{4+} plus vacancies substituting for V^{3+} can explain the observed smaller cell parameter. A crystal-chemical formula in agreement with observed site occupancies is $^{T}(Mg_{0.974})\ ^{M}(V^{3+}_{1.596}\ V^{4+}_{0.316})\ O_4$, with a mean V valence of +3.17. The lattice parameter of the spinel from experiment PC1 is 8.4042(4) Å, smaller than observed for experiment 62504 as expected from its chemistry. In this sample, Fe was detected by microprobe analyses and is assumed to be Fe^{3+} because of the oxidizing synthesis conditions. The T site is then occupied by Mg and Fe^{3+}, as is typically observed in magnetite and magnesioferrite. The crystal-chemical formula consistent with the refinement is $^{T}(Mg_{0.969}\ Fe^{3+}_{0.031})\ ^{M}(V^{3+}_{0.766}\ V^{4+}_{0.602}\ Mg_{0.632})O_4$, with mean V valence of +3.44. The lattice parameters of the $Mg_3(VO_4)_2$ crystal from experiment 92004 are: a = 6.0814(7) Å, b = 11.4686(10) Å, and c = 8.3366(10) Å, which are similar to those previously reported by Krishnamachari and Calvo (1971). The site occupancies were statistically identical to 1.0 after refinement, and therefore they were fixed. The stoichiometry of this phase implies V^{5+}, in agreement with a previous study by Sugiyama et al. (2003).

Measurements of the valence of V were made using synchrotron micro-XANES (X-ray Absorption Near-Edge Structure) spectroscopy (SmX), at the Advanced Photon Source (APS), Argonne National Laboratory (beamline 13-ID, the Consortium for Advanced Radiation Sources or CARS). SmX measurements are made by focusing a monochromatic [cryogenic, Si (111) double-crystal monochromator] X-ray beam (5 × 5 μm) from the synchrotron onto a spot on the sample and measuring the fluorescent X-ray yield from that spot as a function of incident X-ray energy (Table 6). Changes of fluorescent X-ray intensity and energy of features in the XANES spectrum (notably the pre-edge peak) depend on oxidation state and coordination (e.g., Wong et al. 1984). In the present work, the intensity of the XANES pre-edge peak at ~5470 eV was used to determine V oxidation state based on the technique described by Sutton et al. (2005). This method was calibrated using standard basaltic glasses whose V oxidation state has been determined independently by titration and optical spectrometry methods. The oxidation states of V have been inferred using this technique on a range of planetary materials (Karner et al. 2003, 2004, 2006). Although the small size of the X-ray beam is ideal for analyzing small crystals, a few of the oxidized experiments (158B and 202; Table 1) yielded D_V near 0.1. In these cases, the fluorescence of underlying V-rich glass may have interfered with the measurement on spinel, thus resulting in a higher valence for V in spinel. Spinel spectra for both of these samples look similar to that of the glass (especially 158B), so the valence determined for these experiments should be interpreted with caution.

TABLE 2. Spinel compositional data

Exp.	n	TiO_2	RuO_2	Al_2O_3	Cr_2O_3	V_2O_3	FeO t	NiO	MnO	MgO	FeO	Fe_2O_3	Total
FMQ	15	2.15	–	20.99	39.90	0.41(3)	19.07	0.040	n.a.	14.35	14.42	5.17	97.43
+1%V	20	2.37	–	21.02	37.45	3.87(7)	18.88	0.040	n.a.	15.26	13.89	5.55	99.45
+5%V	20	2.39	–	12.96	21.98	24.2(5)	22.33	0.073	n.a.	13.77	14.63	8.55	98.55
+5%Ti	15	4.64	–	19.06	38.42	0.37(3)	19.34	0.063	n.a.	15.59	14.81	5.03	97.98
+10%Ti	15	6.10	–	16.37	38.93	0.33(3)	19.05	0.061	n.a.	15.24	15.58	3.86	96.47
IW+2	20	1.77	–	22.25	39.24	0.37(3)	19.78	0.115	n.a.	13.85	15.12	5.18	97.90
IW	14	2.11	–	27.67	39.24	1.40(6)	15.73	0.033	n.a.	16.66	13.76	2.19	103.06
+1%V	12	3.19	–	18.47	29.88	14.8(4)	18.56	0.042	n.a.	13.54	16.72	2.04	98.68
+5%V	5	3.91	–	10.92	10.39	39.1(6)	20.77	0.030	n.a.	12.13	18.07	3.00	97.55
+5%Ti	17	4.33	–	22.08	39.10	0.96(11)	17.55	0.050	n.a.	14.58	16.68	0.96	98.74
+10%Ti	20	7.99	–	21.93	34.10	2.38(9)	17.16	0.00	n.a.	16.68	16.76	0.44	100.28
IW-1	10	2.20	–	22.10	43.30	1.05(8)	16.22	0.02	0.18	13.99	15.55	0.74	99.13
158A	10	1.67	0.91	9.47	8.46	0.007(1)	49.80	6.73	n.a.	14.94	1.64	53.52	97.35
158B	20	1.14	–	9.84	22.34	0.006(1)	38.10	0.43	n.a.	17.66	3.10	38.90	93.42
159A	7	2.29	–	24.76	31.97	0.15(2)	17.48	1.78	–	18.79	4.06	14.91	98.71
159B	8	2.17	–	16.22	47.33	0.15(2)	11.77	1.95	0.00	18.28	3.48	9.21	98.79
162A	6	2.71	0.12	29.44	23.74	0.14(2)	22.49	0.73	–	15.50	9.92	13.97	96.27
162B	5	3.50	–	22.04	26.61	0.35(4)	30.46	0.03	–	13.32	10.53	22.15	98.53
202	7	0.12	–	2.06	8.83	0.005(2)	63.19	0.32	0.23	12.33	14.57	54.03	97.94
T5-1	10	2.30	–	15.00	34.32	0.29(3)	30.47	0.30	0.38	12.45	15.63	16.49	97.16
T6-1	10	1.56	–	9.08	0.69	0.07(1)	63.39	0.39	0.53	17.02	6.64	63.06	99.04
T11-1	9	1.88	–	12.79	39.28	0.17(2)	30.13	0.57	0.36	12.68	15.05	16.75	99.53
T13-1	10	1.33	–	6.55	1.82	0.04(1)	66.61	0.82	0.27	15.59	8.20	64.91	99.53
T14-1	9	11.55	–	2.67	0.34	0.40(8)	73.27	0.07	0.10	3.82	35.11	42.41	96.47

Notes: n is average of "n" analyses; for major elements, standard deviations of the mean are typically 2% or less; for V the number in parentheses is 2σ error on analysis, FeO t = all Fe calculated as FeO; FeO and Fe_2O_3 calculated according to charge balance and stoichiometry.

TABLE 3. Glass compositional data

Exp.	n	SiO_2	TiO_2	Al_2O_3	Cr_2O_3	V_2O_3	FeO	NiO	MnO	MgO	CaO	Na_2O	K_2O	P_2O_5	Total
FMQ	20	45.41	3.12	12.40	0.13	0.052(11)	11.92	0.01	0.17	11.36	11.76	1.59	0.62	–	98.54
+1%V	7	45.28	3.12	12.09	0.16	0.48(4)	11.61	0.025	0.21	10.94	12.31	1.59	0.58	–	98.40
+5%V	20	44.02	2.81	11.30	0.15	3.86(12)	10.61	0.05	0.19	11.34	11.38	1.75	0.71	–	98.17
+5%Ti	20	43.14	6.58	11.48	0.18	0.06(2)	11.30	0.00	0.20	11.71	11.03	1.74	0.6	–	98.02
+10%Ti	20	41.24	10.82	11.05	0.19	0.06(2)	10.70	0.014	0.18	11.00	10.48	1.85	0.66	–	98.24
IW+2	20	44.78	2.99	11.86	0.15	0.045(15)	13.01	0.01	0.22	12.56	11.45	1.16	0.39	–	98.63
IW	10	43.96	4.16	11.97	0.44	0.076(20)	11.40	0.03	0.20	12.18	11.29	0.69	–	–	96.40
+1%V	10	44.54	3.06	12.10	0.33	0.67(15)	11.42	0.01	0.20	11.92	11.44	0.77	–	–	96.46
+5%V	10	45.09	2.73	11.36	0.17	1.52(12)	10.89	0.01	0.20	12.64	11.26	0.30	–	–	96.17
+5%Ti	10	42.72	6.06	11.74	0.47	0.051(8)	11.77	0.03	0.20	12.11	10.57	0.49	–	–	96.21
+10%Ti	9	39.12	13.62	10.43	0.61	0.12(3)	10.12	0.02	0.17	11.71	9.80	0.69	–	–	96.41
IW-1	15	45.25	2.94	12.04	0.63	0.06(2)	13.80	n.d.	0.20	12.96	11.48	0.17	n.a.	n.a.	99.53
IW-2	20	47.45	3.21	12.91	0.71	0.035(10)	8.76	n.d.	0.22	13.35	12.28	0.05	0.06	n.a.	99.04
158B	10	47.83	3.17	12.45	0.02	0.056(7)	8.96	0.11	–	11.49	12.29	0.42	0.06	0.39	97.25
159A	10	49.20	3.34	13.59	0.13	0.060(9)	5.20	0.18	–	13.15	12.24	1.73	0.59	0.42	99.83
159B	7	52.21	3.36	13.69	0.08	0.049(8)	1.76	0.03	–	12.1	13.01	0.56	0.08	0.49	97.42
162A	10	49.62	3.57	13.15	0.12	0.052(8)	12.51	0.11	–	13.19	3.69	0.22	0.03	0.40	96.66
162B	9	45.37	2.88	11.96	0.18	0.048(7)	11.60	0.11	–	11.52	10.95	1.37	0.50	0.40	96.89
202	10	43.95	2.88	11.94	0.01	0.063(6)	13.73	0.064	0.19	10.85	11.33	1.88	0.42	0.40	97.71
T5-1	5	48.72	1.85	12.41	–	0.026(3)	11.01	0.041	–	9.01	11.08	1.84	0.48	–	96.47
T6-1	10	52.63	2.20	14.31	0.021	0.032(3)	7.45	0.02	0.22	8.15	10.02	2.66	0.78	0.60	99.09
T11-1	5	48.66	2.5	11.43	–	0.026(3)	11.77	0.091	–	10.76	10.96	1.80	0.42	–	98.42
T13-1	5	48.55	2.36	10.92	–	0.024(3)	11.74	0.039	–	11.03	10.22	1.66	0.43	–	96.97
T14-1	9	49.77	2.77	14.79	0.009	0.024(3)	10.22	0.024	0.22	7.42	9.96	2.47	0.70	0.44	98.82

Notes: n is average of "n" analyses; for major elements, standard deviations of the mean are typically 2% or less; for V the number in parentheses is 2σ error on analysis.

TABLE 4. X-ray diffraction data (space group, atomic fractional coordinates, and anisotropic displacement parameters) for the synthetic vanadates

		x	*y*	*z*	*Occ*	U_{11}	U_{22}	U_{33}	U_{12}	U_{23}	U_{13}
62504	T	0.125	= *x*	= *x*	0.974(Mg)	0.00574(24)	= U_{11}	= U_{11}	0	0	0
	M	0.5	= *x*	= *x*	0.956(V)	0.00523(9)	= U_{11}	= U_{11}	–0.00015(3)	= U_{12}	= U_{12}
Fd$\bar{3}$*m*	O	0.26009(9)	= *x*	= *x*		0.00704(25)	= U_{11}	= U_{11}	–0.00050(13)	= U_{12}	= U_{12}
PC1	T	0.125	= *x*	= *x*	0.969(Mg) 0.031(Fe^{3+})	0.00744(56)	= U_{11}	= U_{11}	0	0	0
	M	0.5	= *x*	= *x*	0.684(V) 0.316(Mg)	0.00626(20)	= U_{11}	= U_{11}	0.00012(17)	= U_{12}	= U_{12}
Fd$\bar{3}$*m*	O	0.25994(16)	= *x*	= *x*		0.01056(52)	= U_{11}	= U_{11}	–0.00100(48)	= U_{12}	= U_{12}
92004	Mg1	0	0	0		0.00645(30)	0.01010(20)	0.00539(28)	–0.00110(17)	0	0
	Mg2	0.25	0.13544(3)	0.25		0.00523(20)	0.00710(13)	0.00754(20)	0	–0.00085(15)	0
Cmca	V	0	0.37981(1)	0.12103(2)		0.00501(8)	0.00438(6)	0.00400(8)	0.00007(4)	0	0
	O1	0	0.25145(6)	0.22707(11)		0.00730(39)	0.00684(24)	0.00766(39)	0.00225(21)	0	0
	O2	0	0.00381(6)	0.24426(11)		0.00628(38)	0.00685(23)	0.00525(36)	0.00046(21)	0	0
	O3	0.27293(12)	0.11783(4)	0.99733(8)		0.00724(28)	0.00841(18)	0.00722(28)	–0.00024(15)	0.00095(19)	–0.00088(16)

Notes: Lattice parameters are: a = 8.4110(4) Å for 62504; a = 8.4042(4) Å for PC1; a = 6.0814(7) Å, b = 11.4686(10) Å, c = 8.3366(10) Å for 92004. Each frame was collected for 30 seconds at 45 kV and 40 mA. Intensities were collected to 2θ = 110° for spinels (62504 and PC1) and 90° for $Mg_3(VO_2)_4$ (92004). Corrections for Lorentz polarization and absorption were performed.

TABLE 5. Electron microprobe data for the synthetic vanadates (standard deviation is in parentheses beneath oxide)

Exp.	Phase	MgO	V_2O_3	VO_2	V_2O_5	FeO	Al_2O_3	Total
62304, 62504	MgV_2O_4	21.90 (0.65)	79.50 (0.49)	–	–	–	–	101.40
PC1	Mg_2VO_4	39.23 (0.96)	–	54.92 (0.66)	–	1.79 (0.29)	0.09	96.91
92004	$Mg_3V_2O_8$	37.80 (0.53)	–	–	63.72 (0.52)	–	–	101.52

TABLE 6. Vanadium K XANES results for spinels and coexisting glasses (multiple entries are for replicate analyses)

Exp.	Pre-edge peak Int.	Energy (eV) spinel	valence	Pre-edge peak Int.	Energy (eV) glass	valence
FMQ	89, 69, 76, 90	5470.0, 5470.4, 5469.9, 5469.7	2.97, 2.83, 2.90, 2.97	473	5470.0	4.2
+1%V	102	5469.7	3.05	288	5469.9	3.77
+5%V	167, 165	5469.8, 5469.9	3.36, 3.35	337	5470.0	3.90
+5%Ti	45	5469.3	2.65	240	5469.9	3.62
+10%Ti	50	5469.2	2.68	230	5469.8	3.59
IW+2	57, 68	5469.8, 5469.3	2.75, 2.83	282, 315	5469.8, 5469.3	3.75, 3.84
IW	30, 30, 33	5468.7, 5469.0, 5468.9	2.50, 2.50, 2.52	150, 130	5468.7	3.29, 3.20
+1%V	68	5468.7	2.83	125, 134, 137	5469.2, 5469.3, 5469.1	3.17, 3.22, 3.23
+5%V	77	5468.8	2.90	171	5469.5	3.37
+5%Ti	40	5469.1	2.60	80	5468.3	2.92
+10%Ti	31	5468.8	2.50			
IW-1	30, 33	5467.7, 5468.2	2.49	60, 52	5468.1, 5468.4	2.74
IW-2	–	–	–	145	5468.5	3.27
158B	680, 520	5469.9, 5470.0	4.57, 4.30	670, 710	5470.2, 5470.1	4.56, 4.62
159A	180, 160	5469.4, 5469.8	3.41, 3.33	358	5469.3	3.95
159B	120, 170, 145	5469.5, 5469.7, 5469.7	3.15, 3.37, 3.26	330	5469.7	3.88
162A	130	5468.9	3.19	445	5469.8	4.15
162B	150, 125	5469.7, 5469.5	3.29, 3.17	405	5469.8	4.06
202	180	5469.5	3.41	370	5469.8	3.98
T5	220	5469.7	3.55	760	5470.1	4.70
T6	990		5.00	1100		5.00
T11	350	5470.1	3.94	790	5470.1	4.74
T13	760	5470.4	4.70	790	5470.3	4.74
T14	416	5469.4	4.09	711	5469.4	4.62
MgV_2O_4	103	5469.0	3.05			
$Mg_3V_2O_8$	939	5470.3	4.93			
Cavansite	273		3.72			
Vanadinite	929		4.93			

Linking spinel valence with glasses

Because V in spinel and glass have similar coordination—octahedral under reducing conditions and lower under oxidized conditions—the possibility that the glass calibration of Sutton et al. (2005) is appropriate for spinels was explored. However, measurements on spinels of known V oxidation state are required to calibrate the spinel spectra. To make this comparison, XANES spectra were obtained for the three synthetic oxides described above, as well as for vanadinite (5+) and cavansite (4+). The pre-edge peak intensity obtained on the reduced synthesized spinels (Fig. 3a) is similar to that for glasses containing V^{3+}, as might be expected if the spinel is MgV_2O_4 (Fig. 3b). Similarly, $Mg_3V_2O_8$ contains V^{5+} (Fig. 3a), and

its intensity falls directly on the glass calibration line of Sutton et al. (2005), as do the vanadinite and cavansite intensities (Fig. 3b). This result is similar to the finding of Wong et al. (1984) for spectra acquired for roscoelite and vanadinite. This agreement indicates that the glass calibration line can be applied to the spinel samples of this study (Fig. 3).

Previous XANES studies have found crystallographic orientation effects with some anisotropic minerals. Because spinels are cubic, orientation effects should not be significant. XANES measurements on six different magnetites from a polycrystalline sample equilibrated in a Pt capsule (Magnetite A from study of Righter et al. 2006), yield nearly identical pre-edge peak intensities and energies (Fig. 4). These measurements thus confirm that orientation effects are not significant for spinels and amount to no more than 10% uncertainty in the pre-edge peak intensities.

RESULTS

Equilibrium

Equilibrium between spinel and silicate melt can be assessed by examining the distribution of key major elements between both phases. Compositions of co-existing silicate melt and spinel have been studied extensively by Ariskin and Nikolaev (1996), who derived empirical expressions for partitioning of major elements as a function of T, f_{O_2}, and melt composition. For the new experiments containing Cr-rich spinels, we used the equilibrium partitioning of Cr/Al between spinel and melt and the expression:

$$\ln D_{Cr/Al} = a/T + b \log f_{O_2} + c \ln(Fe^{3+}/Fe^{2+})liq + d(NBO/T) + e \quad (1)$$

where a–e are coefficients from Ariskin and Nikolaev (1996), and NBO/T is calculated according to Mysen (1991). Comparison of calculated and measured $D_{Cr/A}^{spinel/melt}$ for experiments reported in Table 1 show good agreement and suggest that equilibrium was attained in these samples. Additional evidence for an approach to equilibrium in these experiments is the presence of homogeneous, unzoned spinel crystals (Fig. 2).

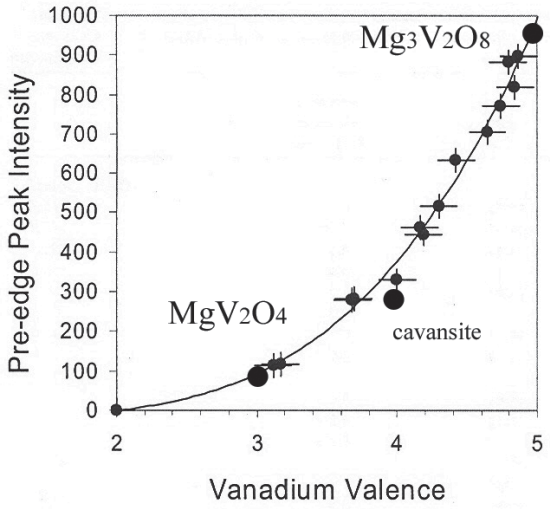

FIGURE 3. Pre-edge intensities measured for MgV_2O_4, Mg_2VO_4, $Mg_3V_2O_8$, and cavansite compared to the glass calibration curve of Sutton et al. (2005). Close correspondence of glass curve with the oxide standards indicates that the glass calibration can be applied to spinels of unknown valence. Intensity is normalized to the value above the absorption edge as described in Sutton et al. (2005).

Spinel V valence always lower than coexisting glass

Micro-XANES spectra, including well defined pre-edge peaks, were obtained on experimental spinels and glasses containing between 50 ppm and 40 wt% V, and in areas as small as 5 × 5 μm. Application of the glass calibration results of Sutton et al. (2005) to the glass pre-edge intensities indicates that glasses equilibrated at FMQ are dominated by V^{4+}, whereas the lowest f_{O_2} glass (IW) contains mixed valence of 4+ and 3+. Glasses in all cases have higher pre-edge intensities (and valence) than the spinel (Fig. 5). The latter was also predicted in the study of Toplis and Corgne (2002) based on thermodynamic calculations.

Spinels grown at reduced conditions have small pre-edge peaks, those grown at intermediate f_{O_2} have intermediate pre-edge peaks, whereas those grown at oxidized conditions have very large pre-edge peaks (Fig. 6). Application of the Sutton et al. (2005) calibration shows that spinels of variable composition grown at oxygen fugacities of FMQ all have similar pre-edge intensities consistent with V^{3+} (Table 6). Spinels grown at higher oxygen fugacities, from FMQ to air, have larger pre-edge peaks that indicate the presence of V^{4+} and V^{5+}. Finally, spinels grown at reduced conditions of IW+2, IW, and IW-1 have a similar or slightly lower intensity (or valence) (Fig. 6). In general, these measurements confirm the suggestions of Canil (1999), who argued for the presence of V^{3+} in $MgAl_2O_4$ spinels, based on experiments in the synthetic system CaO-MgO-Al_2O_3-SiO_2, at oxygen fugacities from NNO to NNO-5. However, there is evidence for both V^{2+} at reducing conditions and V^{4+} and V^{5+} at oxidizing conditions.

The presence of V^{2+} in oxides has been suggested by Connolly and Burnett (2003), based on lower D_V spinel ($MgAl_2O_4$)/melt at the C-CO buffer than at IW (due to the greater affinity of V^{3+} than V^{2+} for the spinel structure). Additionally, Sutton et al. (2002) measured V pre-edge peaks for fassaitic pyroxenes from CAIs in Allende and found evidence for mixed V^{2+} and V^{3+}. It seems likely, then, that at more reduced conditions, divalent V becomes stable in the Cr-rich spinel structure as well.

Another unusual feature of the XANES spectra for spinels in this study is the evidence for V^{5+} in spinels grown at very oxidized conditions. Although only small concentrations of V

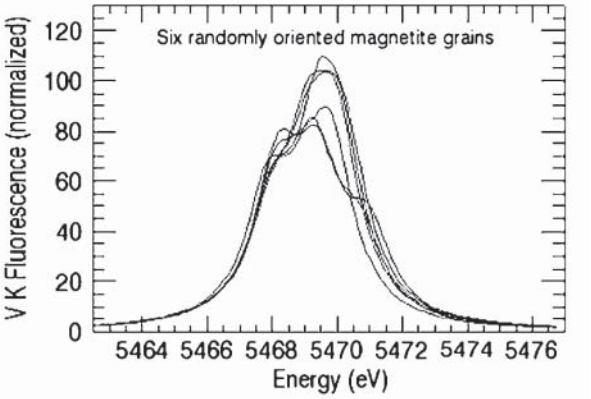

FIGURE 4. Fitted XANES spectra for six spinels of random orientation, illustrating that there is only a small effect of crystallographic orientation on the pre-edge intensities amounting to an uncertainty of 10% in the peak intensities. The spinels are V-bearing magnetites from the study of Righter et al. (2006).

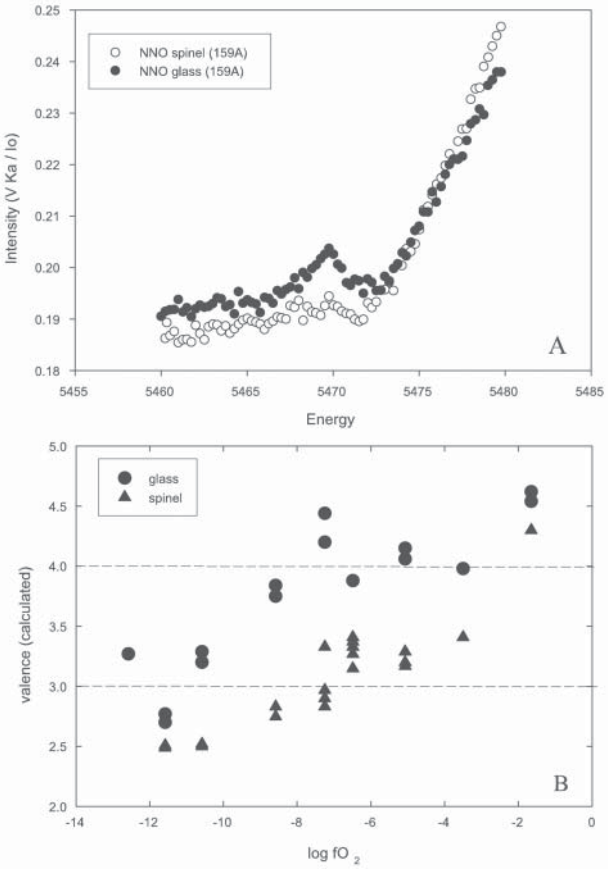

FIGURE 5. (**a**) Pre-edge peak intensities (fitted spectra) for spinel (open circles) and glass (closed circles) equilibrated at the NNO buffer (experiment 159A). (**b**) V valence vs. $\log f_{O_2}$ for all Cr-bearing spinel-glass pairs from this study. All experiments were done at 1300 °C. Vanadium valence was calculated using the glass calibration of Sutton et al. (2005).

are present in these spinels, there is a strong and intense pre-edge peak. Substitution of V^{5+} into the spinel structure requires charge balance with either a 1+ cation or a vacancy. Such spectra have been measured in other materials, such as $LiNiVO_4$ (Liu et al. 2001), $LiCo_xNi_{1-x}VO_4$ (Stallworth et al. 2004), and $Fe_{3-x}V_xO_4$ ($0 < x < 2$) (Nohair et al. 1995), but these are synthetic compounds and were also equilibrated under high oxygen pressures. Because vacancies are not favored in nature and spinels do not contain 1+ cations, V^{5+} is only likely to be present in small amounts in natural systems. It is nonetheless interesting to observe such effects in the spinel structure in oxidized systems.

Differences in V valence in normal vs. inverse spinels that may result from crystal chemical effects, can be evaluated by comparison of results from two different experiments from the study of Leeman (1974), Leeman and Lindstrom (1978), and Righter et al. (2006). Two experiments, one with Cr-bearing spinel (T5; T11) and one with magnetite (T14), were carried out at very similar temperatures and oxygen fugacities. Comparison of the pre-edge peak intensities for these samples shows slightly higher pre-edge intensities for the magnetite than the chromite, indicating that magnetite accepts V^{4+} slightly more than chromite. It is likely that the inverse spinel structure of magnetite favors V^{4+} more so than chromite, as it also true for

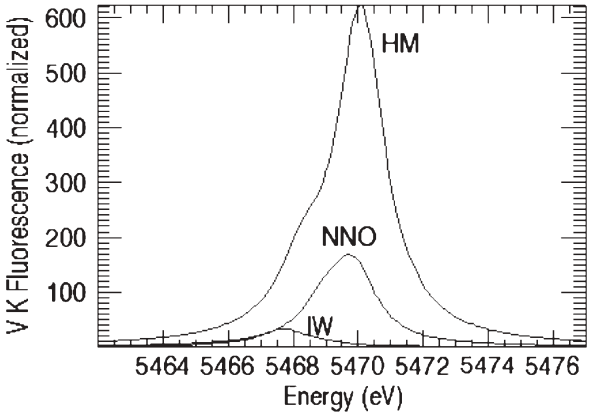

FIGURE 6. Fitted XANES spectra for three different experimental spinels, equilibrated at three different oxygen fugacities—HM (experiment 158A), NNO (experiment 159A), and IW (undoped IW) buffers. Note the increasing intensity of the pre-edge peak with increasing oxygen fugacity.

Ti. This finding illustrates the importance of crystal-chemical control on V partitioning, valence, and solubility in spinels, which should be accounted for in parameterization of partition coefficients for V.

DISCUSSION

Henry's Law and V and Ti content

Previous studies have reported $D_V^{spinel/melt}$ as high as 35, but these were doped with high concentrations of V. Because some variables were not held constant in previous studies, such as Ti content, temperature, and f_{O_2}, it was not clear which variable was providing the strongest control. Therefore, we completed several experiments to isolate these effects, and to try to resolve this question.

Vanadium contents of spinels in the more reduced V-doped experiments are as high as 41 wt% (similar to levels reported by Canil 1997). TiO_2 contents of spinels in the Ti-doped experiments are as high as 8 wt%. Values of $D_V^{spinel/melt}$ range from 5.5 to 8.1 at FMQ and from 18.4 to 25.7 at IW (Fig. 7) and depend upon V and Ti content. For example, a series of experiments at the FMQ buffer with variable V content reveal only little change in $D_V^{spinel/melt}$ with increasing V content of the spinel. However, at the IW buffer, increasing V content of spinel leads to increased D_V from 18.4 to 25.7 (Fig. 7). On the other hand, at both the FMQ and IW buffers, increasing Ti content of the spinels leads to only slightly lower D_V. At FMQ, D_V decreases from 8 to 4.5, and at IW it decreases from 17 to 11. This information, combined with previous work at different temperatures, allows the effect of T, f_{O_2}, and spinel composition on D_V to be evaluated more completely.

The effect of Ti and Fe contents of chromian spinels

Two series of experiments at FMQ and IW were designed to isolate the effect of Ti-content on $D_V^{spinel/melt}$. Although no particular effect was observed on D_V, these experiments also exhibited unexpected behavior with respect to the XANES spectra. As spinel Ti content increases in the experiments at FMQ, the *V* pre-edge peak intensity decreases, at constant temperature and f_{O_2}

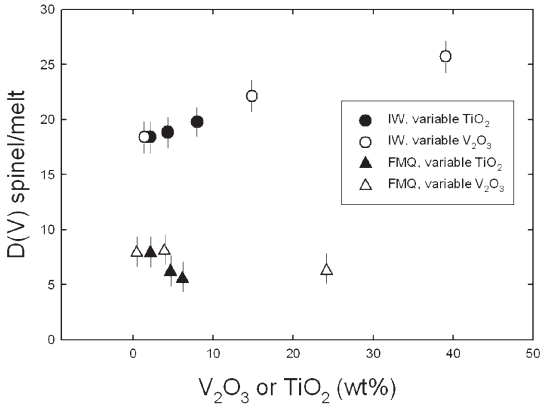

FIGURE 7. D_V vs. V_2O_3 or TiO_2 for experiments at FMQ and IW. Note that D_V increases with increasing V_2O_3 content of the spinel at IW, but stays approximately the same at FMQ-buffered experiments. D_V stays approximately constant with variable TiO_2 content of spinels in IW-buffered experiments, but shows a slight decrease in the FMQ experiments.

(Table 6). This effect is not, however, observed in the IW experiments. The *V* pre-edge intensities are nearly the same despite the increasing Ti content in the spinel, suggesting that Ti does not play a role in the V valence shifts. This behavior may instead be understood in terms of an exchange equilibrium such as $Fe^{2+} + V^{4+} = Fe^{3+} + V^{3+}$, where addition of V^{4+} to the Ti-bearing spinel moves the exchange to the right, thus reducing V compared to Ti-free spinels. This kind of coupled exchange has been observed in glasses (Sutton et al. 2005) and spinels (Papike et al. 2005), and will be considered in later modeling efforts.

Prediction $f(T, f_{O_2}, X)$

It has been clear since the studies of Ringwood and Essene (1970) that $D_V^{spinel/melt}$ is strongly dependent upon f_{O_2}. This trend also was observed and documented by Lindstrom (1976) and Horn et al. (1994), but efforts to predict $D_V^{spinel/melt}$ have not led to straightforward solutions (e.g., Nielsen et al. 1994). It is thus no surprise that the large range of f_{O_2} represented in our spinel/melt experiments (from IW-1 to air) yields a linear trend from $D_V < 1$ to close to 25 (Fig. 8a). This trend is reinforced by a correlation between oxygen fugacity and spinel pre-edge peak intensity (Fig. 8b). In addition, melt composition is known to control partitioning of some elements between minerals and melts (e.g., Ni, Mn, and V in magnetite/melt systems; Toplis and Corgne 2002, and Mn and Zn in olivine/melt systems; Kohn and Schofield 1994). These results, together with the spinel compositional and crystal-chemical effects described above, and the effects of temperature and composition documented in previous studies will be used to derive a predictive expression for $D_V^{spinel/melt}$ for normal spinels (chromite and aluminous spinels) that can be applied to many magmatic situations.

To predict D_V as a function of temperature, oxygen fugacity, and spinel and melt composition, we performed multiple linear regressions on a total of 88 Cr-spinel experiments from this study, as well as from Horn et al. (1994), Canil (1997, 1999), and Righter et al. (2006). Because all four spinel end-members (Ti-, Al-, Cr- and Fe^{3+}-bearing), and melt composition (V and Mg/Si) are potentially important in controlling D_V, we have included terms

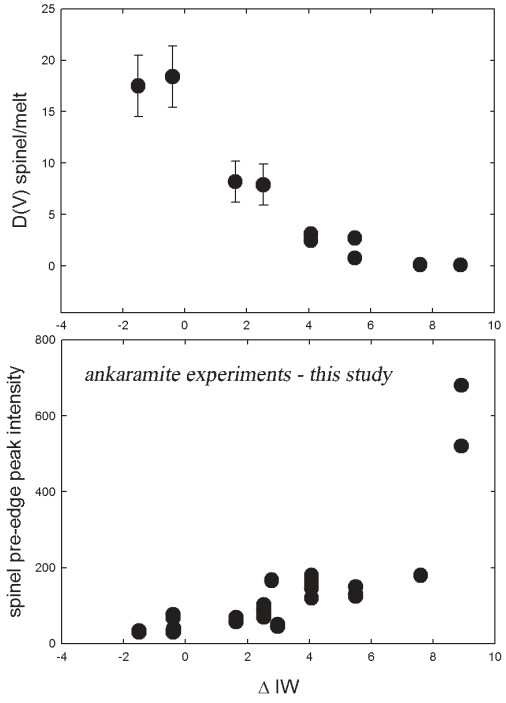

FIGURE 8. (**a**) $D_V^{spinel/melt}$ vs. relative oxygen fugacity [relative to the iron-wüstite (IW) buffer of O'Neill 1987; all experiments done at 1300 °C and with the ankaramite starting composition]; (**b**) Variation of spinel pre-edge peak intensity with oxygen fugacity [again, relative to the iron-wüstite (IW) buffer, 1300 °C];

for each in the linear regression. The equation is of the form:

$$D_V^{spinel/melt} = a/T + b(\log f_{O_2}) + c(X_{Cr}) + d(X_{Fe}^{3+}) + e(X_{Al}) + f(X_{Ti}) + g(V_{melt}) + h(Mg/Si) + i \quad (2)$$

where coefficients a through i were calculated and are presented in Table 7. This expression does not work very well on the entire data set and yields coefficients with large error, as well as a high chi-squared value.

To formulate a better predictive model for $D_V^{spinel/melt}$, we used the results of our XANES measurements that allow identification of regions where the valence of V in spinel is well defined. Because V^{4+} is dominant at oxygen fugacities above the NNO buffer (Fig. 5b), and V^{3+} is dominant at lower than NNO, we performed two different regressions of the dataset: one for oxidized conditions and one for reduced conditions. Comparison of predicted vs. measured D_V (Fig. 9), as well as the smaller coefficient error and chi-squared values (Table 7), demonstrates that the expression effectively captures variation in D_V due to temperature, spinel and melt composition, and oxygen fugacity. This expression was used to calculate $D_V^{spinel/melt}$ relevant to several planetary basalt and mantle suites.

Vanadium depletions in planetary mantles

Siderophile element contents in planetary mantles and derivative melts are controlled by three main processes: the segregation

TABLE 7. Regression parameters for $D_V^{spinel/melt}$

		All expts.		Oxidized >NNO		Reduced <NNO	
Term	constant	value	Std. error	value	Std. error	value	Std. error
1/T	a	16572	1050	−16463	1060	16998	1150
$\log f_{O_2}$	b	−0.208	0.063	−0.828	0.104	−0.213	0.052
X_{Cr}	c	−92.5	12.0	–	–	−98.2	29.2
X_{Fe3+}	d	−97.4	12.1	–	–	−104	30.0
X_{Al}	e	−93.8	12.0	–	–	−99.3	29.1
X_{Ti}	f	−82.7	12.7	–	–	−104	27.6
V in melt (ppm)	g	−0.000085	0.000007	–	–	−0.000102	0.00007
Mg/Si in melt (molar)	h	3.26	1.79	−7.36	2.47	4.09	1.62
	i	81.4	32.1	9.46	7.43	86.6	28.8
N		80		37		49	
X^2		49.5		17.7		13.4	

of a metallic core, magmatic fractionation, and volatility. Because V is refractory and is not affected by volatile processes (e.g., Drake et al. 1989), it is more robust than other slightly siderophile elements such as Mn or Cr (Drake et al. 1989). Typically, the extent to which a siderophile element is depleted in a planetary mantle can be ascertained by comparison with a refractory lithophile element of similar compatibility or incompatibility during melting processes, such as Al or Ti. Titanium has been used by previous workers (e.g., Treiman et al. 1986, 1987), but can be problematic in two ways: First, some lunar basalts have formed by remelting of Ti-rich cumulates. Second, Ti can be much more compatible than V in an evolved magmatic fractionation series (in magnetite). In these two cases, Al is a better choice of a normalizing element. If V is depleted in a mantle that is subsequently melted, there should be a linear array of data on a plot of V vs. Al or Ti. A good example of this behavior is illustrated for the Earth, as V behaves incompatibly in large degrees of partial melting of the terrestrial mantle, as can be seen in the distribution of V in peridotites, komatiites, and komatiitic basalts (Fig. 10). If we had only the komatiitic and basaltic samples in our collections, we could reconstruct the depletion of V with some certainty, as the peridotites and melts lie along the same line.

Because of this, we can use basalts from the Moon, Mars, and Vesta to reconstruct the V content of their mantles, but the effects of magmatic fractionation must be taken into account. Vanadium contents of magmatic samples are typically correlated with indicators of fractionation such as MgO or Al_2O_3 (e.g., MORB, Fig. 12 and lunar basalt, Fig. 11). Although these two magmatic suites from Earth and Moon show the same inverse correlation between V and Al_2O_3, the controlling factors are entirely different. For example, the most primitive MORB samples (Schilling et al. 1983) are those with low V and high Al_2O_3. Subsequent fractionation of plagioclase, olivine, and chromite results in higher V contents and lower MgO and Al_2O_3 contents (Fig. 11). On the other hand, consideration of Apollo 12 and 15 basalt (Taylor et al. 1971; Righter et al. 2000) and picritic glass (Papike et al. 1998) suites illustrates that chromite and olivine fractionation controls transition-element concentrations such as Ni, Co, Cr, and V (Fig. 12). In this case, the most primitive basalt samples start with high V and low Al_2O_3. During fractionation, V contents decrease due to the greater compatibility of V in spinel in this lower oxygen fugacity environment, whereas Al_2O_3 contents increase due to olivine and chromite fractionation. As a result, a trend is produced that is similar to that observed in MORB

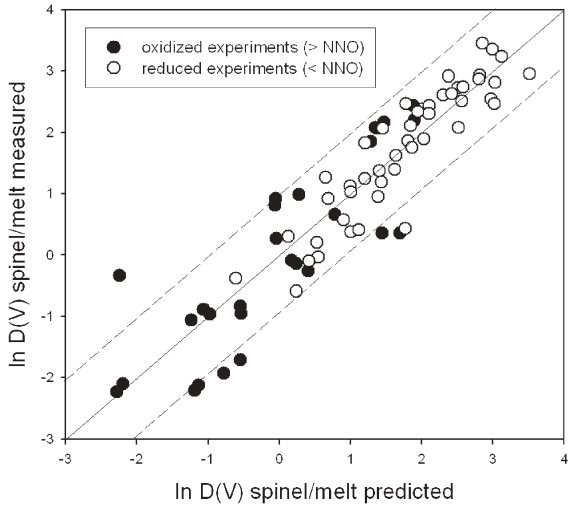

FIGURE 9. Comparison of $D_V^{spinel/melt}$ measured and $D_V^{spinel/melt}$ calculated using Equation 2 and the regression constants from Table 7, for two separate regression calculations: an oxidized subset (n = 37) and a reduced subset (n = 49). Solid line indicates a 1:1 correlation and dashed lines represent 2σ error on the regression; the experimental data were taken from this study and from published experiments (Righter et al. 2006; Horn et al. 1994; Canil 1997, 1999).

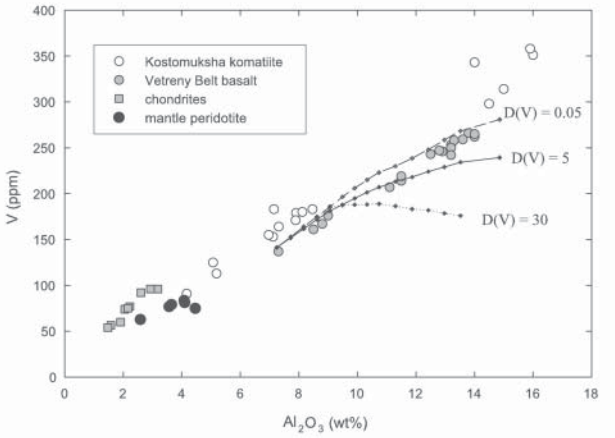

FIGURE 10. V (ppm) vs. Al_2O_3 (wt%) for chondrites (Newsom 1995), peridotites (Jagoutz et al. 1979), and basalts and komatiites from Kostomuksha and the Vetreny Belt (Puchtel et al. 1996, 1998). Also shown are calculated melting trends for $D_V^{spinel/melt}$ = 0.05, 5, and 30, using both Kostomuksha and Vetreny Belt starting compositions and the results of MELTS modeling involving fractionation of olivine and chromite (see Righter et al. 2006).

samples, but in reverse. To reconstruct mantle V content, it is very important to know from which direction the trend originated. This will be illustrated below for the Moon, Mars, and Vesta.

Summary of experimental partitioning data for Vanadium. Although V is usually described as a slightly siderophile element, with a role in core-formation processes, it is also compatible is many mantle and magmatic phases. The recognition of the importance of variables such as temperature, pressure, and melt composition for metal/silicate partitioning led Chabot and Agee (2003) to carry out a systematic study of D_V metal/silicate

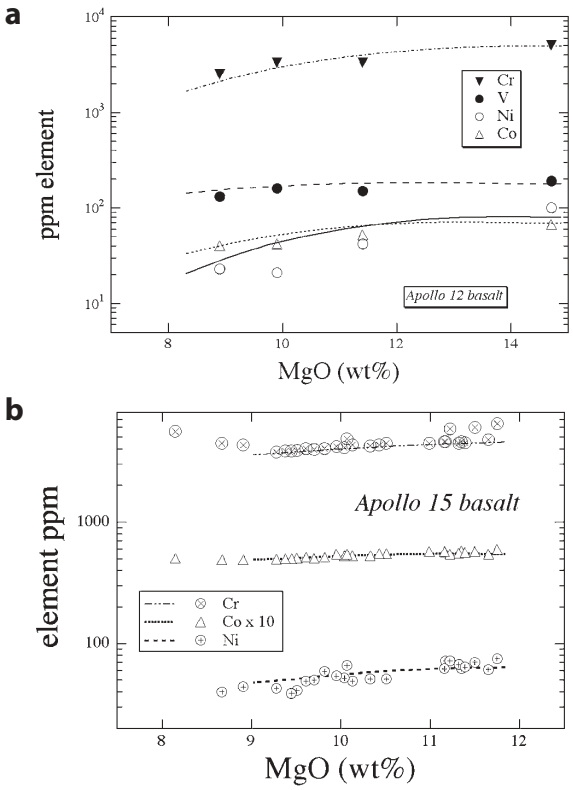

FIGURE 11. (**b**) Correlations between Ni, Co, Cr, and MgO among the Apollo 15 basalt suite (Ryder and Schuraytz 2001). Calculated trends (using MELTS; Ghiorso and Sack 1994) for fractionation at 1 bar, IW buffer, and from 1300 to 1200 °C. The trends shown correspond to fractionation of 8.0% olivine and 1.2% chromite. Calculated Cr contents for this suite were taken from MELTS results. (**a**) Correlations between Ni, Co, V, Cr, and MgO in Apollo 12 basalt samples (data from Taylor et al. 1971). Calculated trends (using MELTS; Ghiorso and Sack 1994) for fractionation at 5 kbar, IW buffer and 1500 to 1200 °C, show that the variation can be ascribed to 31.6% low-Ca pyroxene and 1.6% chromite fractionation. Modeling of both Apollo suites used the following partition coefficients taken from the most reduced experiments of Righter et al. (2006) and basaltic compositions from the compilation of Green (1994): $D_{Ni}^{spinel/melt} = 20$, $D_{Ni}^{olivine/melt} = 8$, $D_{Ni}^{orthopyroxene/melt} = 5$, $D_{Co}^{spinel/melt} = 2$, $D_{Co}^{olivine/melt} = 2$, $D_{Co}^{orthopyroxene/melt} = 2$, $D_{V}^{spinel/melt} = 30$, $D_{V}^{olivine/melt} = 0.1$, $D_{V}^{orthopyroxene/melt} = 1$, $D_{Cr}^{spinel/melt} = 50$, $D_{Cr}^{olivine/melt} = 0.6$, and $D_{Cr}^{orthopyroxene/melt} = 1.5$. The $D_{V}^{spinel/melt} = 30$ was calculated using Equation 2 for the temperature, f_{O_2}, and melt and spinel compositions relevant to the lunar basalt suites (T from MELTS modeling, f_{O_2} at IW-1, chromite with $X_{Cr} = 0.7$, $X_{Al} = 0.2$, and $X_{Ti} = 0.05$, and melt with Mg/Si = 0.5 and 150 ppm V).

at conditions relevant to core formation. Their parameterizations will be used here to compare to silicate and oxide partition coefficients, and also to constrain models for V depletions in several planetary bodies.

Vanadium is compatible and mildly incompatible in some shallow mantle and magmatic phases. For example, plagioclase feldspar, olivine, and orthopyroxene all have $D_V < 1$, but clinopyroxene and spinel both have $D_V > 1$, with the value depending on oxygen fugacity (Fig. 13). A comparison of D_V metal/silicate to D_V "shallow" mantle/melt is made in Figure 13, and illustrates that D_V during mantle melting is higher than that for core formation across a large range of oxygen fugacity. It is only at very low f_{O_2} values that V becomes compatible in metal. Intermediate-depth mantle might consist of majoritic garnet, and wadsleyite or ringwoodite—all of these phases have a slight affinity for V, and a bulk D_V is close to 1 (Fig. 13). Finally, the deep mantle contains Mg-perovskite, Ca-perovskite, and magnesiowüstite. A bulk partition coefficient for the deep mantle is ~2, indicating that the deep mantle is a potential sink for V.

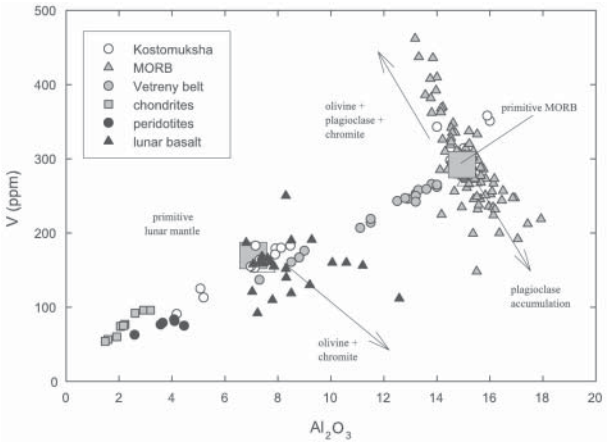

FIGURE 12. V vs. Al_2O_3 for the same data sets as Figure 10, plus mid-ocean ridge basalt (MORB; Schilling et al. 1983) and lunar basalts (from Papike et al. 1998 and compilation in Righter et al. 2000), illustrating the effect of fractionation on V and Al_2O_3 correlations in planetary basalts. During olivine, chromite, and plagioclase fractionation in the relatively oxidized MORB suite, the inverse correlation is caused by the incompatibility of V. During olivine and chromite fractionation in the reduced lunar basalts, the inverse correlation is due to compatibility of V. Shaded boxes represent the primitive mantle-melt compositions for the terrestrial and lunar mantles, taking into account crystal fractionation. From these, the depletions can be estimated.

Earth and Moon. Depletions of V in the Earth and Moon are defined by mantle nodules and high-degree partial melts such as komatiites (Earth) and primitive lunar basalts (Moon). The small depletions of V in the Earth (~80 ppm, Fig. 14; McDonough and Sun 1995) have traditionally been ascribed to either volatility or core formation. More recent studies have focused on the fact that V becomes siderophile at ultra-high temperatures of ~3500 K (e.g., Wade and Wood 2005; Chabot and Agee 2003). However, the deep mantle of the Earth is made of phases in which V is compatible. In fact, the lower mantle (75% of the entire mantle) contains Mg-perovskite, Ca-Perovskite, and magnesiowüstite and given the D_V values discussed above would have a lower mantle/silicate melt bulk partition coefficient of ~2. This alone could account for the depletion of V in the primitive upper mantle. Although V depletions can be accounted for in high P-T scenarios (50 GPa, 3500 K), they can also be accounted for in a relatively low P-T scenario combined with a deep-mantle fractionation (25 GPa, 2500 K; Fig. 15).

The similarity of the V depletion in the Earth and Moon (Fig. 14) has been used by some (e.g., Ringwood et al. 1990) to argue for a common origin for Earth and Moon, or that the impactor core and mantle had equilibrated at high temperatures before the impact with the proto-Earth. Because V deletions are typically small, and can be caused by metal, silicate, or oxide fractions,

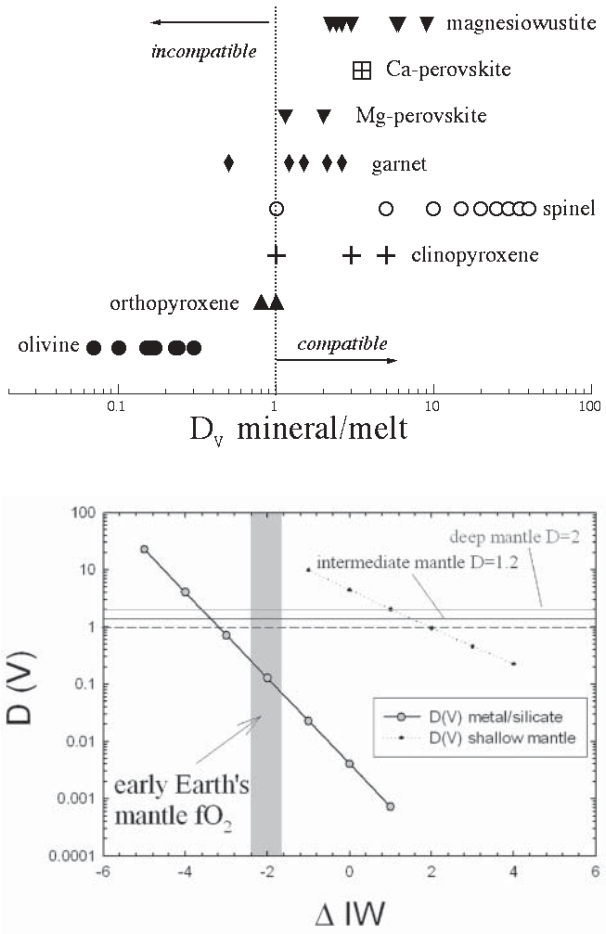

FIGURE 13. Summary of experimental partition coefficients determined in this and previous work. Top histogram: partitioning data from studies of Suzuki and Akaogi (1995, 1998), Gessmann and Rubie (1998), Hauri et al. (1994), Ohtani and Yurimoto (1996), Agee (1993), McFarlane et al. (1994), and McFarlane (1994), Righter et al. (2006), Canil (2001), and compilation of Green (1994). Vertical dashed line represents D_V mineral/melt = 1 or the boundary between compatibility and incompatibility. Bottom diagram: comparison of partition coefficients for V between metal and silicate melt (calculated using the parameterization of Chabot and Agee 2003, for variable oxygen fugacity and fixed temperature, and fixed sulfur and carbon contents of the core (2000 °C, X_S = 0.1, and X_C = 0.1), shallow mantle composed of olivine, orthopyroxene, clinopyroxene, and spinel. Intermediate- and deep-mantle lines (black and gray, respectively) represent the bulk D_V for model terrestrial mantle (Walter et al. 2004). For reference are a shaded region showing the range of f_{O_2} expected for the early Earth, and the dashed horizontal line is D_V = 1.

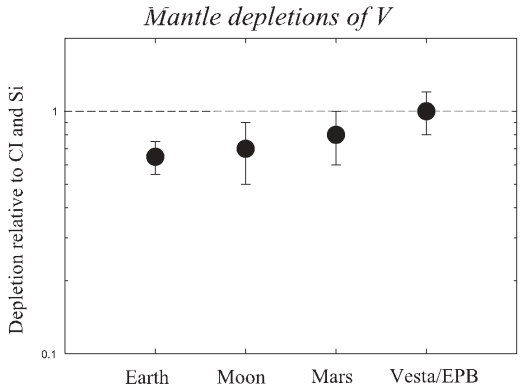

FIGURE 14. Summary of depletions of V in Earth, Moon, Mars, and Vesta, calculated using approaches outlined in the text. Notice that the largest depletions are in the mantles of the Earth and Moon, followed by Mars and Vesta/EPB. Depletions are normalized to CI chondrites and Si, as outlined by Newsom (1995). Horizontal dashed line is that for no depletion.

V may not be the most robust element to distinguish or evaluate various hypotheses for the origin of the Earth and Moon.

Mars. There is some scatter of V and Al for shergottites (perhaps due to grain size effects and heterogeneity), which, together with the notion that Al may be depleted in the martian upper mantle, makes Ti a better normalization element for assessing V depletions in the martian mantle. Consideration of the proposed primitive martian mantle melt, Y980459, which contains 188 ppm V and 0.33 wt% Ti and plots along the terrestrial trend (Fig. 16), suggests a small depletion of V in the martian mantle. This depletion is smaller than the previous estimates of Treiman et al. (1986, 1987) and Dreibus and Wanke (1985), almost certainly due to a larger data set for martian basalts in the intervening 20 years, and filtering out of more evolved samples such as EET 79001 lithology B and Zagami. This assessment shows that V depletions for the martian mantle are slightly higher than the previous estimates of 0.6 (Fig. 14).

Core-formation models of Righter et al. (1998) indicate that Ni, Co, Mo, W, and P contents of the martian mantle can be explained by the presence of a shallow magma ocean (7.5 GPa, 1620 °C, IW-1.4, Xs = mole fraction of sulfur in liquid metal; Fig. 17). Using the parameterization of Chabot and Agee (2003), D_V metal/silicate during core formation under these conditions is ~0.2—not high enough to cause a V depletion (Fig. 17)—and consistent with the lack of depletion evident in the primitive shergottites such as Yamato 980459 (Fig. 16). Furthermore, Mars is distinct from Earth in that the mantle may not be deep enough to stabilize Mg-perovskite. As a result, Mars is too small to have depletions caused by deep-mantle phases, but small V depletions could be caused by intermediate-depth mantle phases such as garnet or ringwoodite.

Vesta (EPB). The eucrite basalts lie far below the V-Al line defined by terrestrial samples, and represent melts of a mantle that potentially has been depleted in V (Fig. 18), due to either core formation or magmatic fractionation. The most widely accepted models for the formation of main group eucrites involve partial melting of, or crystallization from, chondritic starting material that has undergone core formation. For example, Righter and Drake (1997) demonstrated that the concentrations of Ni, Co, Mo, W, and P in the EPB mantle can be explained by segregation of a small core from a CV-L chondrite mixture, at conditions of 1 bar, 1600 °C, IW-2.2, and Xs = 0.20 (Fig. 19). Using the parameterization of Chabot and Agee (2003) for D_V metal/silicate, the concentration of V in such a mantle can be calculated. In that case, D_V is ~0.1, and the concentration of V in the mantle lies above the terrestrial V-Al line and near chondritic

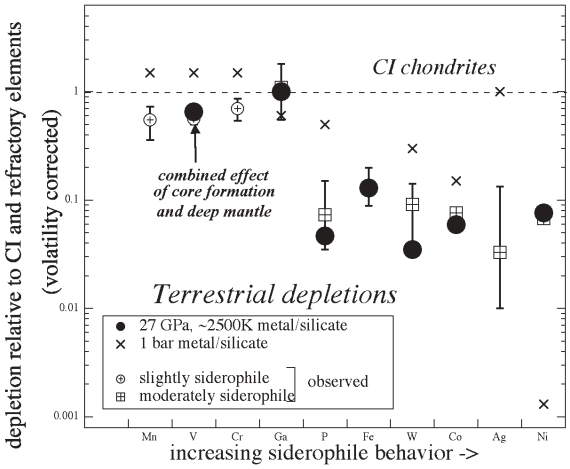

FIGURE 15. Terrestrial depletions of V and other siderophile elements, from the study of Righter and Drake (1999). The calculated value for V is based on a combination of core formation and later mantle fractionation: D_V metal/silicate = 0.2, D_V lower mantle/melt = 2, for lower mantle = 75% of total mantle.

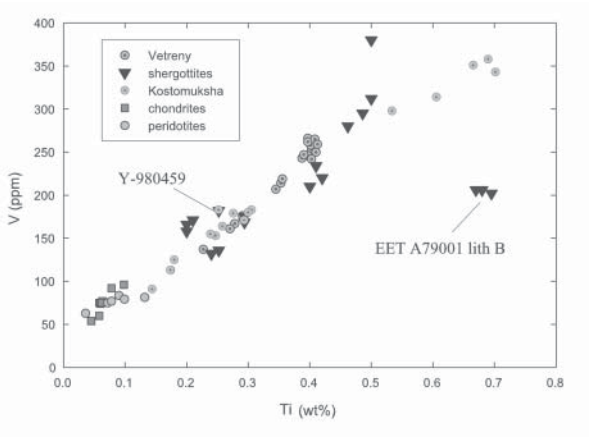

FIGURE 16. V vs. Ti for the same terrestrial samples as Figure 10, plus shergottites (Duke and Silver 1967; Jérome et al. 1970; Smith et al. 1984; Warren et al. 1996; Kong 1999; Dreibus et al. 2000; Zipfel et al. 2000; Neal et al. 2001; Barrat et al. 2002; Jambon et al. 2002; Shirai and Ebihara 2004). Primitive mantle melt composition is best approximated by the olivine phyric shergottite Y980459, which has seen little or no fractionation. From this, the martian mantle V depletion has been estimated. Also note that evolved samples such as EET A79001 lithology B falls off the trend at lower V contents, perhaps reflecting magmatic fractionation.

(Fig. 14). Therefore, the V contents of the eucrites cannot be explained by a depletion event from core formation, and their lower values than the terrestrial line must have been caused by magmatic fractionation.

Crystallization of a model EPB mantle composition after core formation (again a CV-L mixture as advocated by Righter and Drake 1997), shows that during crystallization of chromite, olivine, and orthopyroxene, V decreases while Al is increases (Fig. 18). The lower than terrestrial V contents of the eucrites can be reproduced by equilibrium crystallization of a magma ocean

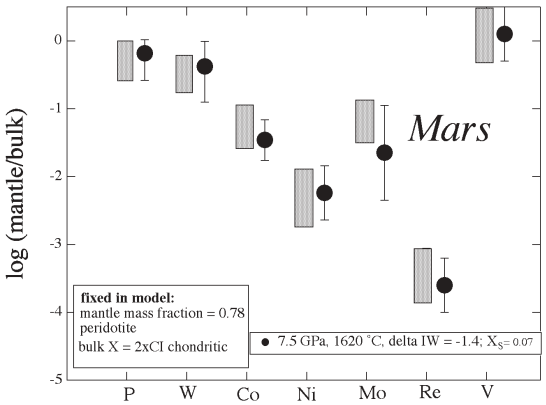

FIGURE 17. Depletions of V as well as Ni, Co, Mo, W, Re, and P for the martian mantle (shaded boxes). The depletions of the latter six elements are fit by Righter et al. (1998) at conditions of shallow metal-silicate equilibrium: 7.5 GPa, 1620 °C, IW-1.4, $X_S = 0.07$, with peridotite melt and a core 22% of the mass of Mars.

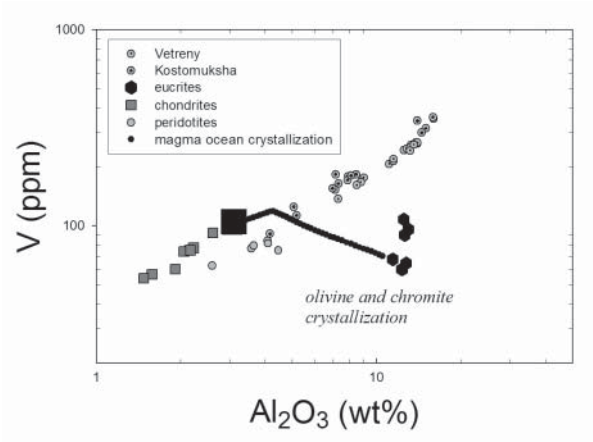

FIGURE 18. V vs. Al_2O_3 for the same terrestrial and chondritic datasets as Figure 10, plus eucrites (from Fukuoka et al. 1977; Warren et al. 1996). Calculated trend (using MELTS; Ghiorso and Sack 1994) is for equilibrium crystallization of the 70% L-30% CV mantle composition after core formation of Righter and Drake (1997). This liquid was cooled from 1600 °C, at 1 bar and the IW buffer. During the cooling, olivine (61%), pyroxene (12%), and chromite (1.1%) crystallize, and V contents of the liquid were calculated using $D_V^{spinel/melt} = 35$, $D_V^{olivine/melt} = 0.1$, and $D_V^{orthopyroxene/melt} = 1$ (the latter two from the compilation of Green 1994). The $D_V^{spinel/melt} = 35$ was calculated using Equation 2 for the temperature, f_{O_2}, and melt and spinel compositions relevant to Vesta/EPB model mantle melts and eucrite basalt suites (T from MELTS modeling, f_{O_2} at IW-2, chromite with $X_{Cr} = 0.75$, $X_{Al} = 0.21$, $X_{Ti} = 0.04$, and melt with Mg/Si = 0.4 and 100 ppm V).

(Fig. 19), which also produces the Ni, Co, Mo, W, and P contents of eucrites as demonstrated by Righter and Drake (1997).

SUMMARY STATEMENT

These new results show that the valence of V in spinels is always lower than in the coexisting melt. Also, the new results together with previously published results show that $D_V^{spinel/melt}$ can be predicted as a function of temperature, f_{O_2}, and spinel and

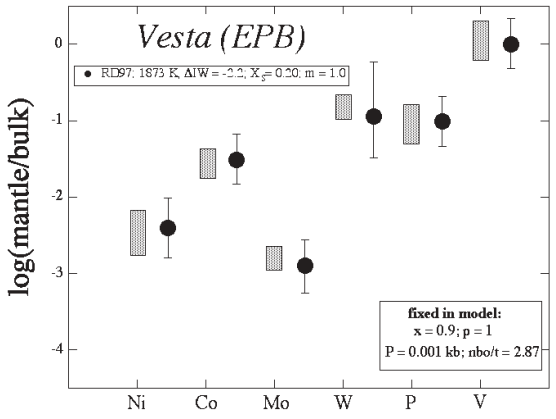

FIGURE 19. Depletions of V as well as Ni, Co, Mo, W, and P for the EPB mantle (shaded boxes). The depletions of the latter five elements were fit by Righter and Drake (1997) at conditions of metal-silicate equilibrium for a CV-L bulk composition that experienced core segregation (0.1 mass fraction of the asteroid) at 1 bar, 1600 °C, IW-2.2, and $X_S = 0.20$. The calculated depletion for V is based on the metal/silicate partitioning parameterization of Chabot and Agee (2003), resulting in a D_V metal/silicate = 0.1 for these conditions; this low D_V does not produce a depletion of V in the Vesta/EPB mantle.

melt composition. Finally, V depletions in planetary mantles can be caused by core formation, magmatic fractionation, and mantle fractionation, and must be interpreted differently in each individual case, rather than in a generalized way.

ACKNOWLEDGMENTS

Presentation of the ideas and interpretation of the results has benefited from discussions with D. Canil, N. Chabot, H. Connolly, L. Grossman, R. Hervig, J. Jones, J. Karner, W. Leeman, J. Papike, C. Shearer, and S. Simon. The journal reviews of M. Toplis and T. Labotka improved the manuscript substantially. K. Domanik helped to verify electron microprobe analyses and L. Danielson provided assistance with some of the XANES measurements. This research is supported by a NASA RTOP to K. Righter.

REFERENCES CITED

Agee, C.B. (1993) High-pressure melting of carbonaceous chondrite. Journal of Geophysical Research, 98, 5419–5426.

Ariskin, A.A. and Nikolaev, G.S. (1996) An empirical model for the calculation of spinel-melt equilibria in mafic igneous systems at atmospheric pressure: 1. chromian spinels. Contributions to Mineralogy and Petrology, 123, 282–292.

Barrat, J.A., Jambon, A., Bohn, M., Gillet, Ph., Sautter, V., Gopel, C., Lesourd, M., and Keller, F. (2002) Petrology and chemistry of the Picritic Shergottite North West Africa 1068 (NWA 1068). Geochimica et Cosmochimica Acta, 66, 3505–3518.

Borisov, A.A., Kadik, A.A., Zharkova, Ye.V., and Kalinichenko, N.V. (1987) Effects of oxygen fugacity on the ratio between valency forms of vanadium in magmas. Geokhimiya, 7, 915–920.

Canil, D. (1997) Vanadium partitioning and the oxidation state of Archaean komatiite magmas. Nature, 389, 842–845.

——— (1999) Vanadium partitioning between orthopyroxene, spinel, and silicate melt and the redox states of mantle source regions for primary magmas. Geochimica et Cosmochimica Acta, 63, 557–572.

——— (2002) Vanadium in peridotites, mantle redox, and tectonic environments: Archean to present. Earth and Planetary Science Letters, 195, 75–90.

Capobianco, C.J. and Drake, M.J. (1990) Partitioning of ruthenium, rhodium, and palladium between spinel and silicate melt and implications for platinum group element fractionation trends. Geochimica et Cosmochimica Acta, 54, 869–874.

Capobianco, C.J., Hervig, R.L., and Drake, M.J. (1994) Experiments on crystal/liquid partitioning of Ru, Rh, and Pd for magnetite and hematite solid solutions crystallized from silicate melt. Chemical Geology, 113, 23–43.

Carmichael, I.S.E. (1967) Iron-titanium oxides and oxygen fugacity in volcanic rocks. Journal of Geophysical Research, 72, 4665–4687.

Chabot, N.L. and Agee, C.B. (2003) Core formation in the Earth and Moon: new experimental constraints from V, Cr, and Mn. Geochimica et Cosmochimica Acta, 67, 2077–2091.

Connolly, H.C., Jr. and Burnett, D.S. (2003) On Type B CAI formation: Experimental constraints on f_{O2} variations in spinel minor element partitioning and reequilibration effects. Geochimica et Cosmochimica Acta, 67, 4429–4434.

Drake, M.J., Newsom, H.E., and Capobianco, C.J. (1989) V, Cr, and Mn in the Earth, Moon, EPB, and SPB and the origin of the Moon: experimental studies. Geochimica et Cosmochimica Acta, 53, 2101–2111.

Dreibus, G. and Wanke, H. (1985) Mars, a volatile-rich planet. Meteoritics, 20, 367–381.

Dreibus, G., Spettel, B., Haubold, R., Jochum, K.P., Palme, H., Wolf, D., and Zipfel, J. (2000) Chemistry of a New Shergottite: Sayh Al Uhaymir 005. Meteoritics and Planetary Science Supplement, 35, A49.

Duke, M.B. and Silver, L.T. (1967) Petrology of eucrites, howardites, and mesosiderites. Geochimica et Cosmochimica Acta, 31, 1637–1642.

Fukuoka, T., Boynton, W.V., Ma, M.S., and Schmitt, R.A. (1977) Genesis of howardites, diogenites, and eucrites. Proceedings of the 8th Lunar Science Conference, 1, 187–210.

Gessmann, C.K. and Rubie, D.C. (1998) The effect of temperature on the partitioning of nickel, cobalt, manganese, chromium, and vanadium at 9 GPa and constraints on formation of the Earth's core. Geochimica et Cosmochimica Acta, 62, 867–882.

Ghiorso M.S. and Sack R.O. (1994) Chemical mass transfer in magmatic processes IV. A revised an internally consistent thermodynamic model for the interpolation and extrapolation of liquid-solid equilibria in magmatic systems at elevated temperatures and pressures. Contributions to Mineralogy and Petrology, 119, 197–212.

Green, T.H. (1994) Experimental studies of trace element partitioning applicable to igneous petrogenesis-Sedona 16 years later. Chemical Geology, 117, 1–36.

Hauri, E.H., Wagner, T.P., and Grove, T.L. (1994) Experimental and natural partitioning of Th, U, Pb, and other trace elements between garnet, clinopyroxene, and basaltic melts. Chemical Geology, 117, 149–166.

Horn, I., Foley, S.F., Jackson, S.E., Jenner, G.A. (1994) Experimentally determined partitioning of high field strength and selected transition elements between spinel and basaltic melt. Chemical Geology, 117, 193–218.

Jagoutz, E., Palme, H., Baddenhausen, H., Blum, K., Cendales, M., Dreibus, G., Spettel, B., Lorenz, V., and Wanke, H. (1979) The abundances of major, minor and trace elements in the earth's mantle as derived from primitive ultramafic nodules. Proceedings of the 10th Lunar and Planetary Science Conference, 2031–2050.

Jambon, A., Barrat, J.A., Sautter, V., Gillet, Ph., Göpel, C., Javoy, M., Joron, J.L., and Lesourd, M. (2002) The basaltic shergottite Northwest Africa 856 (NWA 856): Petrology and chemistry. Meteoritics and Planetary Science, 37, 1147–1164.

Jérome, D.Y. (1970) Composition and origin of some achondrite meteorites. Ph.D. dissertation, University of Oregon.

Karner, J.M., Sutton, S.R., Papike, J.J., Shearer, C.K., and Newville, M. (2003) Oxidation State of Vanadium in Glass and Olivine from Terrestrial and Martian Basalts: Implications for Oxygen Fugacity Estimates. Proceedings of the 34th Annual Lunar and Planetary Science Conference, abstract no. 1998.

Karner, J.M., Sutton, S.R., Papike, J.J., Delaney, J.S., Shearer, C.K., Newville, M., Eng, P., Rivers, M., and Dyar, M.D. (2004) A New Oxygen Barometer for Solar System Basaltic Glasses Based on Vanadium Valence. Proceedings of the 35th Lunar and Planetary Science Conference, abstract no. 1269.

Karner, J.M., Sutton, S.R., Papike, J.J., Shearer, C.K., Jones, J.H., and Newville, M. (2006) Application of a new vanadium valence oxybarometer to basaltic glasses from the Earth, Moon, and Mars, American Mineralogist, 91, 270–277.

Kohn, S.C. and Schofield, P.F. (1994) The importance of melt composition in controlling trace element behavior: An experimental study of Mn and Zn partitioning between forsterite and silicate melts. Chemical Geology, 117, 73–87.

Kong, P. (1999) Siderophile elements in Martian meteorites and implications for core formation in Mars. Geochimica et Cosmochimica Acta, 63, 1865–1875.

Krishnamachari, N. and Calvo, C. (1971) Refinement of the structure of $Mg_3(VO_4)_2$. Canadian Journal of Chemistry, 49, 1629–1637

Leeman, W.P. (1974) Experimental determination of the partitioning of divalent cations between olivine and basaltic liquid, Pt. II, p. 231–337. Ph.D. thesis, University of Oregon.

Leeman, W.P. and Lindstrom, D.J. (1978) Partitioning of Ni^{2+} between basaltic and synthetic melts and olivine-an experimental study. Geochimica et Cosmochimica Acta, 42, 800–816.

Lindstrom, D.J. (1976) Experimental study of the partitioning of the transition metals between clinopyroxene and coexisting silicate liquids. Ph.D. thesis, University of Oregon.

Liu, R.S., Cheng, Y.C., Gundakaram, R. and Jang, L.Y. (2001) Crystal and electronic structures of inverse spinel-type $LiNiVO_4$. Materials Research Bulletin, 36, 1479–1486.

Mamiya, H. and Onoda, M. (1995) Electronic states of vanadium spinels MgV_2O_4 and ZnV_2O_4. Solid State Communications 95, 217–221.

Maurel, C. and Maurel, P. (1983) Étude expérimentale de l'équilibre Fe^{2+}-Fe^{3+} dans les spinelles chromifères et les liquides silicatés basiques coexistants, à 1 atm.

Comptes Rendus de l'Académie des Sciences, 295, 209–212.
McDonough, W.F. and Sun, S.-s. (1995) The composition of the Earth. Chemical Geology, 120, 223–253.
McFarlane, E.A. (1994) Differentiation in the early Earth: An experimental investigation, 153 p. Ph.D. thesis, University of Arizona.
McFarlane, E.A., Drake, M.J., and Rubie, D.C. (1994) Element partitioning between Mg-perovskite, magnesiowüstite, and silicate melt at conditions of the Earth's mantle. Geochimica et Cosmochimica Acta, 58, 5161–5172.
Mysen, B.O. (1991) Relations between structure, redox equilibria of iron, and properties of magmatic liquids. In L.L. Perchuk and I. Kushiro, Eds., Physical Chemistry of Magmas, p. 41–98. Springer-Verlag, New York.
Neal, C.R., Taylor, L.A., Ely, J.C., Jain, J.C., and Nazarov, M.A. (2001) Detailed Geochemistry of New Shergottite, Dhofar 019. Proceedings of the 32nd Annual Lunar and Planetary Science Conference, abstract no. 1671.
Newsom, H.E. (1995) Composition of the solar system, planets, meteorites, and major terrestrial reservoirs. In T.J. Ahrens, Ed., Global Earth Physics: A Handbook of Physical Constants, AGU Reference Shelf, 1, p. 159–89. American Geophysical Union, Washington, D.C.
Nielsen, R.L., Forsythe, L.M., Gallahan, W.E., and Fisk, M.R. (1994) Major- and trace-element magnetite-melt equilibria. Chemical Geology, 117, 167–191.
Nohair, M., Aymes, D., Perriat, P., and Gillot, B. (1995) Infrared spectra-structure correlation study of vanadium-iron spinels and of their oxidation products. Vibrational Spectroscopy, 9, 181–190.
Ohtani, E. and Yurimoto, H. (1996) Element partitioning between metallic liquid, magnesiowüstite and silicate liquid at 20 GPa and 2500 °C: a SIMS study. Geophysical Research Letters, 23, 1993–1996.
O'Neill, H.St.C. (1987) Quartz-fayalite-iron and quartz-fayalite-magnetite equilibria and the free energy of formation of fayalite and magnetite. American Mineralogist, 72, 67–75.
Papike, J.J., Ryder, G., and Shearer, C.K. (1998) Lunar samples. In J.J. Papike, Ed., Planetary Materials, 36, p. 5-1–5-234. Reviews in Mineralogy, Mineralogical Society of America, Chantilly, Virginia.
Papike, J.J., Karner, J.M., and Shearer, C.K. (2005) Comparative planetary mineralogy: valence state partitioning of Cr, Fe, Ti, and V among crystallographic sites in olivine, pyroxene, and spinel from planetary basalts. American Mineralogist, 90, 277–290.
Pouchou, J.-L. and Pichoir, F. (1991) Quantitative analysis of homogeneous or stratified microvolumes applying the model "PAP". In K.F.J. Heinrich and D.E. Newbury, Eds., Electron Microprobe Quantitation, p. 31–75. Plenum Press, New York.
Puchtel, I.S., Hofmann, A.W., Mezger, K., Shchipansky, A.A., Kulikov, V.S., and Kulikov, V.V. (1996) Petrology of a 2.41 Ga remarkably fresh komatiitic basalt lava lake in Lion Hills, central Vetreny Belt, Baltic Shield. Contributions to Mineralogy and Petrology, 124, 273–290.
Puchtel, I.S., Brügmann, G.E., and Hofmann, A.W. (1998) Precise Re-Os mineral isochron and Pb-Nd-Os isotope systematics of a mafic-ultramafic sill in the 2.0 Ga Onega plateau (Baltic Shield). Earth and Planetary Science Letters, 170, 447–461.
Reuter, B., Aust, R., Colsmann, G., and Neuwald, C. (1983) Darstellung und eigenschaften vanadium(II)-haltiger und damit n-leitender vanadium(III)-spinelle. Zeitschrift für Anorganische und Allgemeine Chemie, 500, 188–198.
Righter, K. and Drake, M.J. (1997) A magma ocean on Vesta: core formation and petrogenesis of eucrites and diogenites. Meteoritics and Planetary Science, 32, 929–944.
——— (1999) Effect of water on metal-silicate partitioning of siderophile elements: A high pressure and temperature terrestrial magma ocean and core formation. Earth and Planetary Science Letters, 171, 383–399.
Righter, K., Hervig, R.L., and Kring, D. (1998) Accretion and core formation in Mars: Molybdenum contents of melt inclusion glasses from three SNC meteorites. Geochimica et Cosmochimica Acta, 62, 2167–2177.
Righter, K., Walker, R.J., and Warren, P.H. (2000) Significance of Highly Siderophile Elements and Osmium Isotopes in the Lunar and Terrestrial Mantles. In R.M. Canup and K. Righter, Eds., Origin of the Earth and Moon, p. 291–322. University of Arizona Press, Tucson.
Righter, K., Campbell, A.J., Humayun, M., and Hervig, R.L. (2004) Partitioning of Re, Ir, Rh, and Ru between Cr-bearing spinel, olivine, pyroxene, and silicate melts. Geochimica et Cosmochimica Acta, 68, 867–880.
Righter, K., Leeman, W.P., and Hervig, R.L. (2006) Partitioning of Ni, Co, and V between spinel-structured oxides and silicate melts: Importance of spinel composition. Chemical Geology, 227, 1–25.
Ringwood, A.E. and Essene, E.J. (1970) Petrogenesis of Apollo 11 basalts, internal constitution, and origin of the Moon. Proceedings of the Apollo 11 Lunar Science Conference, 769–799.
Ringwood, A.E., Kato, T., Hibberson, W., and Ware, N. (1990) High-pressure geochemistry of Cr, V, and Mn and implications for the origin of the Moon. Nature, 347, 174–176.
Roeder, P.L. and Reynolds, I. (1991) Crystallization of chromite and chromium solubility in basaltic melts. Journal of Petrology, 32, 909–934.
Rüdorff, W. and Reuter, B. (1947) Die struktur der magnesium- und zink-vanadinspinelle. Zeitschrift für Anorganische und Allgemeine Chemie, 253 194–208.
Ryder, G. and Schuraytz, B. (2001) Chemical variation of the large Apollo 15 olivine normative mare basalt rock samples. Journal of Geophysical Research, 106, 1435–1451.
Schilling, J.-G., Zajac, M., Evans, R., Johnston, T., White, W., Devine, J.D., and Kingsley, R. (1983) Petrologic and geochemical variations along the mid-Atlantic Ridge from 29 to 73° N. American Journal of Science, 283, 510–586.
Sheldrick, G.M. (1997) SHELX97 and SHELXS97. University of Göttingen, Germany.
Shirai, N. and Ebihara, M. (2004) Chemical characteristics of a martian meteorite, Yamato 980459. Antarctic Meteorite Research, 17, 55–67.
Smith, M.R., Laul, J.C., Ma, M.-S., Huston, T., Verkouteren, R.M., Lipschutz, M.E. and Schmitt, R.A. (1984) Petrogenesis of the SNC (shergottites, nakhlites, chassignites) meteorites-Implications for their origin from a large dynamic planet, possibly Mars. Proceedings of the 14th Lunar and Planetary Science Conference, Journal of Geophysical Research, Supp. 89, B612–B630.
Snetsinger, K.G., Bunch, T.E., and Keil, K. (1968) Electron microprobe analysis of vanadium in the presence of titanium. American Mineralogist, 53, 1770–1773.
Stallworth, P.E., Guo, X., Tatham, E., Greenbaum, S.G., Arribito, M., Bodoarado, S., and Penazzi, N. (2004) A solid state ^{51}V NMR characterization of vanadium sites in $LiCo_xNi_{1-x}VO_4$. Solid State Ionics, 170, 181–186.
Sugiyama, S., Hashimoto, T., Shigemoto, N., and Hayashi, H. (2003) Redox behaviors of magnesium vanadate catalysts during the oxidative dehydrogenation of propane. Catalysis Letters, 89, 229–233.
Sutton, S.R., Simon, S., Grossman, L., Delaney, J.S., Beckett, J., Newville, M., Eng, P., and Rivers, M. (2002) Evidence for Divalent Vanadium in Allende CAI Fassaite and Implications for Formation Conditions. Lunar and Planetary Science, XXXIII, abstract no. 1907.
Sutton, S.R., Karner, J., Papike, J.J., Delaney, J.S., Shearer, C.K., Newville, M., Eng, P., Rivers, M., and Dyar, M.D. (2005) Vanadium *K*-edge XANES of synthetic and natural basaltic glasses and applications to microscale oxygen barometry. Geochimica et Cosmochimica Acta, 69, 2333–2348.
Suzuki, T. and Akaogi, M. (1995) Element partitioning between olivine and silicate melt under high pressure. Physics and Chemistry of Minerals, 22, 411–418.
——— (1998) Element partitioning between some mantle minerals and the coexisting silicate melt under pressure. In M. Manghnani and T. Yagi, Eds., Properties of Earth and Planetary Materials at High Pressure and Temperature. AGU Geophysical Monograph, 101, 261–270.
Taylor, S.R., Rudowski, R., Muir, P., Graham, A., and Kaye, M. (1971) Trace element chemistry of lunar samples from the Ocean of Storms. Proceedings of the 2nd Lunar Science Conference, 1083–1091.
Toplis, M.J. and Corgne, A. (2002) An experimental study of element partitioning between magnetite, clinopyroxene, and iron-bearing silicate liquids with particular emphasis on vanadium. Contributions to Mineralogy and Petrology, 144, 22–37.
Treiman, A.H., Drake, M.J., Janssens, M.-J., Wolf, R., and Ebihara, M. (1986) Core formation in the Earth and shergottite parent body (SPB)—Chemical evidence from basalts. Proceedings of the 16th Lunar and Planetary Science Conference, Geochimica et Cosmochimica Acta, 50, 1071–1091.
Treiman, A.H., Jones, J.H., and Drake, M.J. (1987) Core formation in the shergottite parent body and comparison with the earth. Proceedings of the 17th Lunar and Planetary Science Conference, Journal of Geophysical Research, 92, E627–E632.
Wade, J. and Wood, B.J. (2005) Core formation and the oxidation state of the Earth. Earth and Planetary Science Letters. 236, 78–95.
Walter, M.J., Nakamura, E., Tronnes, R.G., and Frost, D.J. (2004) Experimental constraints on crystallization differentiation in a deep magma ocean. Geochimica et Cosmochimica Acta, 68, 4267–4284.
Warren, P.H., Kallemeyn, G.W., Arai, T., and Kaneda, K. (1996) Compositional-petrologic investigation of eucrites and the QUE94201 shergottite. Antarctic Meteorites, XXI, 195–197.
Wong, J., Lytle, F.W., Messmer, R.P., and Maylotte, D.H. (1984) *K*-edge absorption spectra of selected vanadium compounds. Physical Review B (Condensed Matter), 30, 5596–5610.
Zipfel, J., Scherer, P., Spettel, B., Dreibus, G., and Schultz, L. (2000) Petrology and chemistry of the new shergottite Dar al Gani 476. Meteoritics and Planetary Science, 35, 95–106.

MANUSCRIPT RECEIVED OCTOBER 3, 2005
MANUSCRIPT ACCEPTED MAY 10, 2006
MANUSCRIPT HANDLED BY THEODORE LABOTKA